

Two-exciton states and spectroscopy of phenylacetylene dendrimers

Vladimir Chernyak, Evgeni Y. Poliakov, Sergei Tretiak, and Shaul Mukamel

Department of Chemistry, University of Rochester, Rochester, New York 14627

(Received 14 May 1999; accepted 3 June 1999)

The two-exciton wave functions of conjugated dendrimers with fractal geometries are calculated using the Frenkel-exciton model. Self-similarity and the high degree of symmetry make it possible to express the two-photon spectra of these chromophore aggregates in a compact form using irreducible representations of optical excitations, single-exciton states, and an effective two-exciton transition dipole moment. The explicit calculation of the complete manifold of two-exciton states which involves an expensive $l^3 \times l^3$ diagonalization, l being number of generations, is totally avoided. A real space analysis shows that the two-exciton states and resonances are dominated by periphery chromophores due to their exponentially large number. © 1999 American Institute of Physics. [S0021-9606(99)00133-6]

I. INTRODUCTION

Dendrimers made out of phenylacetylene oligomer segments connected through metasubstitutions of the benzene rings¹⁻³ constitute an interesting class of conjugated polymers whose self-similar Cayley tree (Bethe lattice) geometry²⁻⁵ leads to unusual transport and optical properties (Fig. 1).

Two families of such dendrimers have been synthesized in a search for artificial antenna systems that mimic biological energy transfer processes:^{1,6-8} compact dendrimers, which have the same linear unit (segment) in all generations, and extended dendrimers with varying segment length, which decreases toward the periphery. This paper focuses on the first five members of the compact family depicted in Fig. 1. The dependence of the absorption spectra on the number of generations for these two families suggests that optical excitations are localized on the linear segments.² This conjecture has been confirmed by a theoretical study⁹ which showed that optical excitations in dendrimers do not involve charge separation between different segments but merely allow for coherent energy transfer.⁹ These studies lead to the following picture of electronic excitations: The linear segments can be considered as effective chromophores where the elementary excitations reside, whereas the Coulomb coupling between chromophores causes coherent energy transfer which can result in the delocalization of excitations over the entire molecule. Stated differently, the relative motion of a photogenerated electron-hole pair is confined to a single chromophore (linear segment), whereas its center of mass can move across the entire molecule.

Such excitations, known as Frenkel excitons,^{10,11} are usually used to describe the optical properties of a variety of systems which can be modeled as collections of coupled chromophores with nonoverlapping charge distributions, e.g., molecular crystals,^{10,11} nanostructures,¹² J -aggregates,¹³ and core light-harvesting antennae complexes such as LH1 and LH2.¹⁴ The optical response of these systems can be computed using the Frenkel-exciton Hamiltonian,¹⁰⁻¹²

$$H = \sum_{\bar{n}} \Omega_{\bar{n}} B_{\bar{n}}^{\dagger} B_{\bar{n}} + \sum_{\bar{n} \neq \bar{m}} J_{\bar{n}\bar{m}} B_{\bar{m}}^{\dagger} B_{\bar{n}} - \varepsilon(t) \sum_{\bar{m}} \mu_{\bar{m}} (B_{\bar{m}}^{\dagger} + B_{\bar{m}}), \quad (1)$$

where we label the chromophores by Latin indices with an overbar. $B_{\bar{m}} (B_{\bar{m}}^{\dagger})$ are the annihilation (creation) operators of an excitation localized on the \bar{m} -th chromophore which satisfy the commutation relations

$$[B_{\bar{n}}, B_{\bar{m}}^{\dagger}] = \delta_{\bar{n}\bar{m}} (1 - 2B_{\bar{m}}^{\dagger} B_{\bar{m}}), \quad (2)$$

$$[B_{\bar{n}}, B_{\bar{m}}] = [B_{\bar{n}}^{\dagger}, B_{\bar{m}}^{\dagger}] = (B_{\bar{m}}^{\dagger})^2 = (B_{\bar{m}})^2 = 0. \quad (3)$$

$\Omega_{\bar{n}}$ represents the electronic transition energy of the \bar{n} -th chromophore. The Coulomb interaction between chromophores results in the hopping matrix elements $J_{\bar{n}\bar{m}}$. Typically, $|J_{\bar{n}\bar{m}}| \ll \Omega_{\bar{n}}$, and the eigenstates of the Frenkel-exciton Hamiltonian therefore form well-separated manifolds of n -exciton states (see Fig. 2) which are only coupled by the driving field $\varepsilon(t)$ through the third term in Eq. (1). This implies that the linear optical response is solely determined by one-exciton states whereas multiexciton states can be probed by nonlinear optical techniques.¹²

The one-exciton states and the linear response of dendrimers were calculated in our earlier work.⁵ We have further studied the third-order optical spectra using a method based on the exciton scattering matrix which avoids the diagonalization of the two-exciton Hamiltonian.¹⁵ In this paper we study the two-exciton states which dominate the two-photon absorption and certain four-wave mixing signals of dendrimers. The relevant-level scheme, which includes the ground state and two manifolds (bands) of one- and two-exciton states, is shown in Fig. 2. We use Greek indices with an overbar ($\bar{\alpha}$) and a tilde ($\tilde{\alpha}$) to label the one-exciton and two-exciton states, respectively. The one- and two-exciton manifold bandwidths are of the order of the interchromophore coupling J which is much smaller than the transition frequency Ω . If the detunings of incoming fields ω_1 and ω_2 from the one-exciton band are large compared to its bandwidth, the signal becomes independent of the detailed

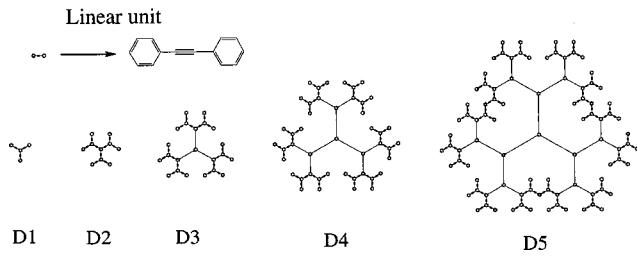


FIG. 1. Structures of the compact phenylacetylene dendrimers family made of the same linear unit.

properties of one-exciton states. The signal can therefore be described by an effective model which only includes the ground state and the two-exciton manifold.

In Sec. II we express the four-wave mixing signal in terms of the two-exciton wave functions $\Psi(\bar{m}, \bar{n})$. These can be found by diagonalizing the two-exciton Hamiltonian. The two-exciton states which participate in the four-wave mixing signal are classified in Appendix C. For l generations, there are $N^{(2)} = l(l^2 + 4l + 1)/6$ two-exciton states. To avoid the diagonalization of a huge $N^{(2)} \times N^{(2)}$ matrix, we use an indirect method for computing the two-exciton eigenstates based on comparing the expression for the nonlinear signal in terms of the two-exciton states with the one that uses the exciton scattering matrix. In Sec. III we apply this approach to dendrimers. In Sec. IV we present numerical calculations of the two-exciton wave functions which dominate the two-photon spectroscopy. A brief summary of our results is given in Sec. V.

II. TWO-PHOTON SPECTROSCOPY OF CHROMOPHORE AGGREGATES

In our previous work,¹⁵ the nonlinear signal which does not depend on dendrimer geometry has been computed using the exciton scattering matrix approach. To interpret the signal in terms of the two-exciton states we first express the signal in terms of the two-exciton wave functions $\Psi_{\bar{\alpha}}$.

To avoid interference between one- and two-exciton resonances and minimize the dependence of the signal on dendrimer geometry, we follow Ref. 15 and consider a frequency-domain two-color heterodyne detected four-wave mixing signal generated by three incoming beams \mathbf{k}_1 , \mathbf{k}_2 , and \mathbf{k}_3 with $\omega_3 = \omega_1$ with polarizations $\hat{e}_1, \hat{e}_2, \hat{e}_3$ in the direction $\mathbf{k}_s = \mathbf{k}_1 + \mathbf{k}_2 - \mathbf{k}_3$. Tuning ω_1 and ω_2 to be off-resonant with respect to the one-exciton manifold while keeping $\omega_1 + \omega_2$ on resonance with the two-exciton band allows us to study the two-exciton states alone, avoiding the

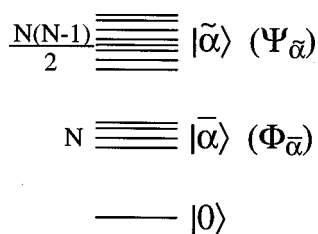


FIG. 2. Manifolds of one- and two-exciton states in phenylacetylene dendrimers.

influence of one-exciton resonances. By choosing the polarization direction of the heterodyne field, $\hat{e}_s = \hat{e}_3$, and incoming fields, $\hat{e}_1 = \hat{e}_2$, and averaging over all possible directions of \hat{e}_3 and \hat{e}_2 , we eliminate the signal's dependence on geometry.¹⁵

The two-color four-wave mixing signal is given by¹⁵

$$S(\omega_1, \omega_2) \propto \text{Im}[\hat{\chi}^{(3)}(-\omega_2; \omega_1, \omega_2, -\omega_1)]. \quad (4)$$

In Appendix A, we express the third-order optical susceptibility $\hat{\chi}^{(3)}$ in terms of the one- and two-exciton eigenstates, $\phi_{\bar{\alpha}}$ and $\Psi_{\bar{\alpha}}$. Averaging over orientations of \hat{e}_1 and \hat{e}_3 and evaluating the matrix elements of effective polarization operator $P_{\text{eff}}^{(j)}$ [see Eq. (A5)] by making use of Eqs. (1)–(3) in Eq. (A3), we obtain

$$S(\omega_1, \omega_2) = \frac{1}{(\omega_1 - \Omega)^4} \sum_{\bar{\alpha}} d_{\bar{\alpha}}^2(\omega) \frac{\gamma}{(\omega - \epsilon_{\bar{\alpha}})^2 + \gamma^2}. \quad (5)$$

Here $\omega = \omega_1 + \omega_2$, Ω is an average single-exciton energy, and

$$d_{\bar{\alpha}}(\omega) = (\omega - 2\Omega) \sum_{\bar{m}\bar{n}} \Psi_{\bar{\alpha}}(\bar{m}, \bar{n}) - 2 \sum_{\bar{m}\bar{n}\bar{k}} \Psi_{\bar{\alpha}}(\bar{m}, \bar{n}) J_{\bar{n}\bar{k}} \quad (6)$$

is an effective transition dipole, where the two-exciton wave function is given by

$$|\bar{\alpha}\rangle = \sum_{\bar{m}\bar{n}} \Psi_{\bar{\alpha}}(\bar{m}, \bar{n}) B_{\bar{m}}^{\dagger} B_{\bar{n}}^{\dagger} |g\rangle. \quad (7)$$

Without loss of generality, Ψ is taken to be symmetric: $\Psi_{\bar{\alpha}}(\bar{m}, \bar{n}) = \Psi_{\bar{\alpha}}(\bar{n}, \bar{m})$, and $\Psi_{\bar{\alpha}}(\bar{m}, \bar{m}) = 0$. Equations (5)–(7) represent the signal as a sum of resonances whose positions correspond to the two-exciton state energies, whereas the effective oscillator strengths $d_{\bar{\alpha}}^2(\omega_{\bar{\alpha}})$ are determined by the two-exciton wave functions $\Psi_{\bar{\alpha}}$.

Equations (5) and (6) express the signal for any aggregate described by the Frenkel-exciton Hamiltonian in terms of the two-exciton wave functions. The two-exciton states which dominate the signal can be computed by diagonalizing the two-exciton Hamiltonian derived in Appendix C and applying Eqs. (5) and (6). However, this numerically expensive procedure can be avoided, similar to how the nonlinear optical response is expressed in terms of the frequency-dependent exciton scattering matrix $\bar{\Gamma}(\omega)$, avoiding the explicit computation of the two-exciton states.^{12,16} To express the two-exciton states in terms of the exciton scattering matrix we introduce the two-exciton variables

$$Y_{\bar{m}\bar{n}}(\omega) = \int d\tau \exp(i\omega\tau) \langle B_{\bar{m}}(\tau) B_{\bar{n}}(\tau) \rangle. \quad (8)$$

Here $B(\tau)$ is the Heisenberg operator in the optically driven system to first order in the field. It can be calculated in two ways. First, it can be expanded in terms of the two-exciton wave functions using a standard procedure.¹² Alternatively, $Y_{\bar{m}\bar{n}}(\omega)$ can be computed using the scattering matrix approach. Comparing the two expressions for $Y_{\bar{m}\bar{n}}(\omega)$ provides a convenient method to compute two-exciton eigenstates.

In Appendix A we show that two-exciton coherence $Y_{\bar{m}\bar{n}}$ is proportional to two-exciton wave function $\Psi_{\bar{\alpha}}(\bar{m}, \bar{n})$ provided the two-exciton dephasing rate γ is smaller than the spacing between the two-exciton levels,

$$\Psi_{\bar{\alpha}}(\bar{m}, \bar{n}) = \frac{\gamma(\omega_1 - \Omega)^2}{d_{\bar{\alpha}}(\omega)} \text{Im}[Y_{\bar{m}\bar{n}}(\omega_{\bar{\alpha}})], \quad (9)$$

where $Y_{\bar{m}\bar{n}}$ is given by (B2).

We have employed Eq. (9) to calculate $\Psi_{\bar{\alpha}}(\bar{m}, \bar{n})$ using the following steps. We first compute the signal at high resolution, e.g., $\gamma \rightarrow 0$. [For this, we use the frequency-dependent exciton scattering matrix $\bar{\Gamma}_{\bar{m}\bar{n}}$ and one-exciton wave functions and energies from Eqs. (24) and (29) in Ref. 15]. We then calculate $\text{Im}[Y_{\bar{m}\bar{n}}(\omega)]$ from Eqs. (B3)–(B6) by using $\bar{\Gamma}_{\bar{m}\bar{n}}$ and the one-exciton states for those frequencies, which correspond to the strongest resonances of $S(\omega_1, \omega_2)$, e.g., at $\omega_1 + \omega_2 = \omega_{\bar{\alpha}}$. This yields the wave functions of the two-exciton states which dominate the signal. As the dephasing rate is increased, the peaks are no longer resolved, and $Y_{\bar{m}\bar{n}}(\omega)$ at the peak values of ω represent the superpositions of the several two-exciton wave functions which can be considered as the relevant collective variables.

We conclude the section by establishing a relation which allows us to interpret the signal in terms of $Y_{\bar{m}\bar{n}}(\omega)$. It follows from Eqs. (5), (6), and (B1) that the signal can be recast in a doorway–window representation in real space,

$$S(\omega_1, \omega_2) = \frac{1}{(\omega_1 - \Omega)^2} \sum_{\bar{m}\bar{n}} \text{Im}[M_{\bar{m}\bar{n}}(\omega) Y_{\bar{m}\bar{n}}(\omega)]. \quad (10)$$

Here Y serves as a doorway created by the incoming fields, and the window function is

$$M_{\bar{m}\bar{n}}(\omega) = (\omega - 2\Omega - i\gamma) - \sum_k (J_{\bar{m}\bar{k}} + J_{\bar{n}\bar{k}}). \quad (11)$$

Along with Eq. (9) this implies that the contribution of each pair of chromophores to a given resonance is equal to the values of the corresponding wave function $\Psi_{\bar{\alpha}}(\bar{m}, \bar{n})$ weighted by the window function $M_{\bar{m}\bar{n}}(\omega)$.

III. THE TWO-EXCITON STATES

In this section we apply the approach of Sec. II to compute the two-exciton wave functions which dominate the four-wave mixing and the pump–probe signals in compact phenylacetylene dendrimers.

The dendrimer is modeled as an assembly of coupled two-level chromophores, each representing a linear segment. Only nearest-neighbor coupling, i.e., between segments which are attached to the same phenyl ring, is important. The nearest-neighbor approximation produces the coupling pattern represented by the dual Bethe lattices shown in Fig. 3. The absolute magnitude of the coupling is the same for all nearest neighbors $|J| = 67 \text{ cm}^{-1}$; the signs of the coupling constants are given by the following rule: $J > 0 (J < 0)$ for two chromophores of the same (different) generation.⁵

In our earlier work we have related the linear optical response of compact dendrimers to the properties of one-

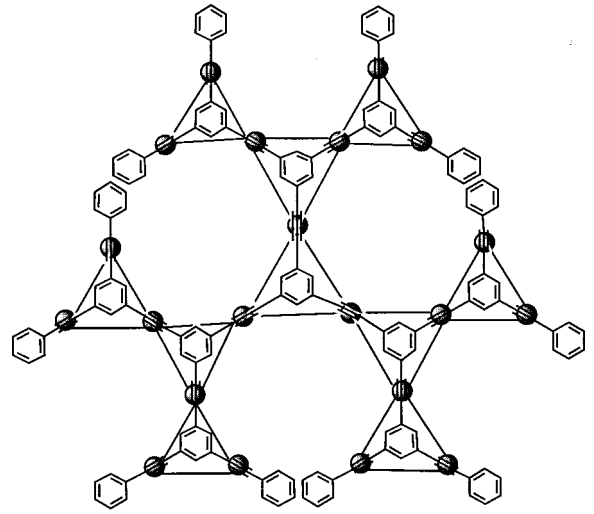


FIG. 3. Dual Bethe lattice with triangular cycles representing nearest-neighbor interactions.

exciton states.⁵ The high symmetry made it possible to determine all one-exciton states, thereby mapping the calculation of one-exciton states in a dendrimer with l generations (Dl) onto a much simpler effective linear-chain problem with chain length not exceeding l . The two-photon spectra have been calculated as well¹⁵ by applying the exciton-scattering picture of the nonlinear optical response.^{12,16} The scattering matrix $\bar{\Gamma}(\omega)$ was represented in terms of components related to irreducible representations of the dendrimer symmetry group G_l . Computation of the exciton scattering matrix is reduced to inverting of $l \times l$ matrices.¹⁵

The expression for the two-exciton wave functions [Eq. (9)] involves the scattering matrix and the one-exciton wave functions [Eq. (B2)]. All one-exciton states in dendrimers are partitioned into two classes: antisymmetric and symmetric.⁵ The antisymmetric excitons are classified by their length $s = 1, 2, \dots, l-1$ and the quantum number $\alpha = 1, \dots, s$. They are characterized by their energies $\epsilon_{\alpha}^{(s)}$ and auxiliary wave functions $\psi_{\alpha}^{(s)}(m)$ with $m = 1, \dots, s$. The symmetric excitons are classified by the quantum numbers $\alpha = 1, \dots, l$ and $t = 1, 2, 3$ as well as characterized by the energies $\epsilon_{\alpha,t}$ and auxiliary wave functions $\tilde{\psi}_{\alpha}^{(t)}(m)$, with $m = 1, \dots, l$. Expressions for $\epsilon_{\alpha}^{(s)}$, $\epsilon_{\alpha,t}$, $\psi_{\alpha}^{(s)}(m)$, and $\tilde{\psi}_{\alpha}^{(t)}(m)$ are given in Ref. 5.

Following Refs. 5 and 15, we denote the set of chromophores (linear segments) for a compact dendrimer Dl by X_l and the symmetry group by G_l . We reiterate that the chromophores $\bar{m} \in X_l$ are denoted with overbarred Latin indices. It follows from Eq. (6) that the effective dipole operator $d_{\bar{\alpha}}(\omega)$ of a two-exciton state $\bar{\alpha}$ is obtained by calculating the overlap of its wave function with the window function $M_{\bar{m}\bar{n}}$ [Eq. (11)]. Since the window function is symmetric with respect to the dendrimer symmetry group G_l , only those two-exciton states which are symmetric with respect to G_l contribute to the signal. This implies that $Y_{\bar{m}\bar{n}}(\omega)$ is symmetric as well.

The two-exciton quantities [e.g., $Y_{\bar{m}\bar{n}}(\omega)$] which are symmetric with respect to G_l can be conveniently described by introducing the intersection point, $\bar{p}(\bar{i}, \bar{j})$, of the chro-

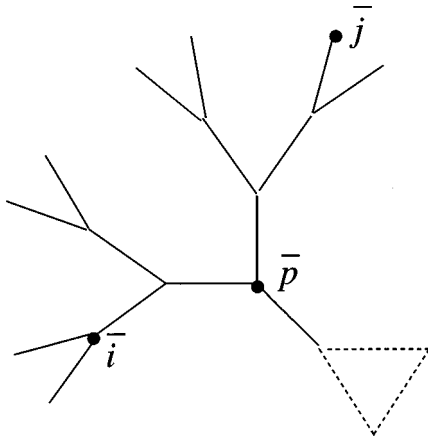


FIG. 4. Definition of the intersection point $\bar{p}(\bar{i}, \bar{j})$ of the chromophores \bar{i} and \bar{j} . \bar{p} is the first intersection of the unique paths leading from \bar{i} and \bar{j} to the center. Any symmetric two-exciton quantity, e.g., $Y_{\bar{i}\bar{j}}$, can be labelled by $|\bar{i}|$, $|\bar{j}|$, and $|\bar{p}(\bar{i}, \bar{j})|$.

mophores \bar{i} and \bar{j} , defined as follows. On a Bethe lattice, which can be obtained from dual Bethe lattice (Fig. 3) by eliminating the connections within the same generations, there is a unique path from each chromophore to the center. For two chromophores \bar{i} and \bar{j} we define $\bar{p}(\bar{i}, \bar{j})$ to be the first chromophore where the two paths of \bar{i} and \bar{j} intersect as shown in Fig. 4. If the two paths do not intersect, we set $\bar{p} = 0$. $Y_{\bar{i}\bar{j}}$ can thus be parameterized by a three-index matrix $Y_{ij,p}$, where $i = |\bar{i}|$, $j = |\bar{j}|$, and $p = |\bar{p}(\bar{i}, \bar{j})|$. $|\bar{m}|$ denotes the generation number where \bar{m} resides in the dendrimer. Stated differently, the matrix elements of the symmetric matrix are equal, $Y_{\bar{i}\bar{j}} = Y_{\bar{i}'\bar{j}'}$, provided $|\bar{i}| = |\bar{i}'|$, $|\bar{j}| = |\bar{j}'|$, and $p = p'$. $Y_{ij,p}$ describes $n_{ij,p}$ equivalent chromophore pairs (\bar{i}, \bar{j}) where the degeneracy factors $n_{ij,p}$ are given by

$$\begin{aligned} n_{ij,0} &= 3 \cdot 2^{i+j}, & n_{ii,0} &= 3 \cdot 2^{2i-1}, \\ n_{ii,p} &= 3 \cdot 2^{2(i-1)-p}, & n_{ij,j} &= 3 \cdot 2^i, \\ n_{ij,p} &= 3 \cdot 2^{i+j-p-1}, & 0 < p &\leq \min\{i, j\}. \end{aligned} \quad (12)$$

These quantities are plotted in Fig. 5. We observe that degeneracy increases exponentially toward the periphery.

$Y_{ij,p}(\omega)$ can be obtained starting with Eq. (B2), which can be simplified considerably by utilizing the symmetry. The first $\bar{\Gamma}_{\bar{m}\bar{n}}(\omega)$ enters Eq. (B2) through the combinations $\Sigma_{\bar{n}} \bar{\Gamma}_{\bar{m}\bar{n}}(\omega)$; the latter only depends on $|\bar{m}|$ and is given by $\bar{\Gamma}_m(\omega)$ with $m = |\bar{m}|$. $\bar{\Gamma}_m(\omega)$ has been computed in Ref. 15.

Using Eqs. (12) and (B3)–(B7), we finally recast Eq. (10) in the form

$$\begin{aligned} S(\omega_1, \omega_2) &= \frac{1}{(\omega_1 - \Omega)^2} \sum_{ij,p} n_{ij,p} \\ &\times \text{Im}[M_{ij,p}(\omega_1 + \omega_2) Y_{ij,p}(\omega_1 + \omega_2)]. \end{aligned} \quad (13)$$

As seen from Eq. (9), the imaginary part of two-exciton coherence $\text{Im}(Y_{ij,p})$ determines two-exciton wave function $\Psi_{\bar{\alpha}}(ij,p)$ when $\gamma \rightarrow 0$. The overlap of $Y_{ij,p}$ with the window function $M_{ij,p}$ [Eq. (13)] determines the two-photon signal.

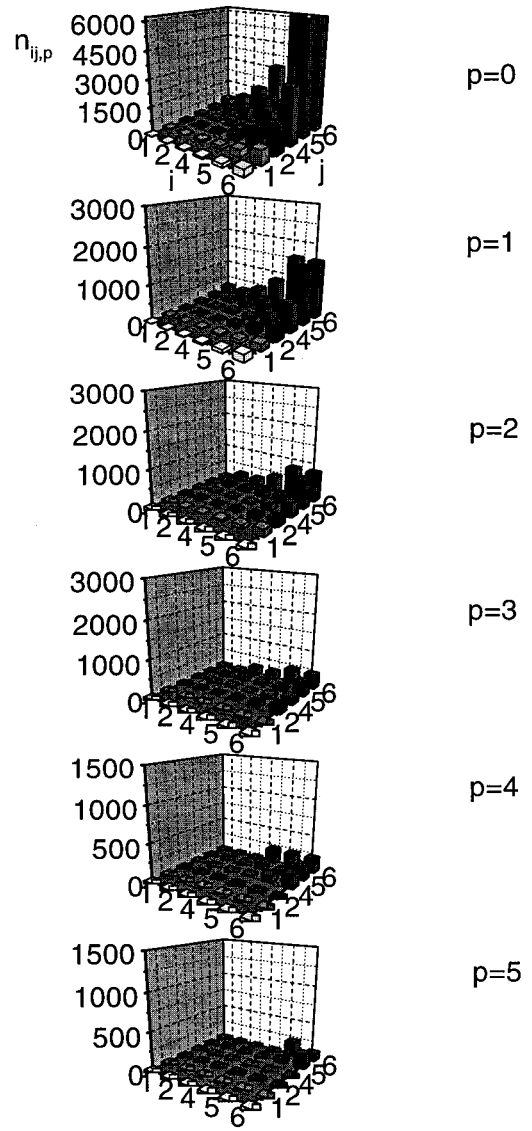


FIG. 5. Degeneracy factors $n_{ij,p}$ [Eq. (12)] for equivalent chromophore pairs (i, j) of D_6 .

In the next section we use this equation to analyze the various contributions from distinct chromophores to the signal.

IV. NUMERICAL CALCULATIONS

The computed two-photon absorption $S(\omega_1, \omega_2)$ is plotted in Fig. 6 as a function of the sum-frequency detuning from the two-exciton resonance, $\Delta\omega = \omega_1 + \omega_2 - 2\Omega$ with one-exciton dephasing rate $\gamma = 3 \text{ cm}^{-1}$. The five strongest two-exciton resonances in D_6 appear at $\Delta\omega \approx -105, -35, 120, 340, 420 \text{ cm}^{-1}$. The absorption signal saturates with the number of generations, and the low-resolution spectra ($\gamma \sim 15 \text{ cm}^{-1}$) of D_5 and D_6 shown in Fig. 7 are virtually identical. Hereafter we focus on D_6 .

The entire two-exciton wave function $\Psi_{\bar{\alpha}}(ij,p)$ for the strongest ($\Delta\omega \approx 120 \text{ cm}^{-1}$) resonance is displayed in Fig. 8(a). The wave function has both positive and negative values. These are displayed separately in the left and the right

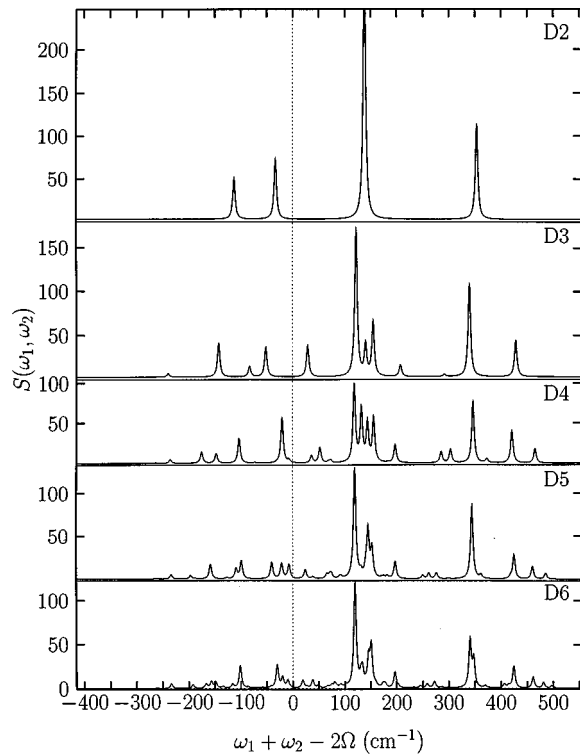


FIG. 6. Calculated two-photon spectra of D2-D6 with two-exciton dephasing rate $\gamma \sim 3 \text{ cm}^{-1}$.

columns, respectively. Each panel shows $\Psi_{\bar{\alpha}}(ij,p)$ versus i and j for a given p . p varies between 0 to 5: $p=0$ represents chromophores of different branches whereas $p=1, \dots, 5$ represent two chromophores of the same branch which must

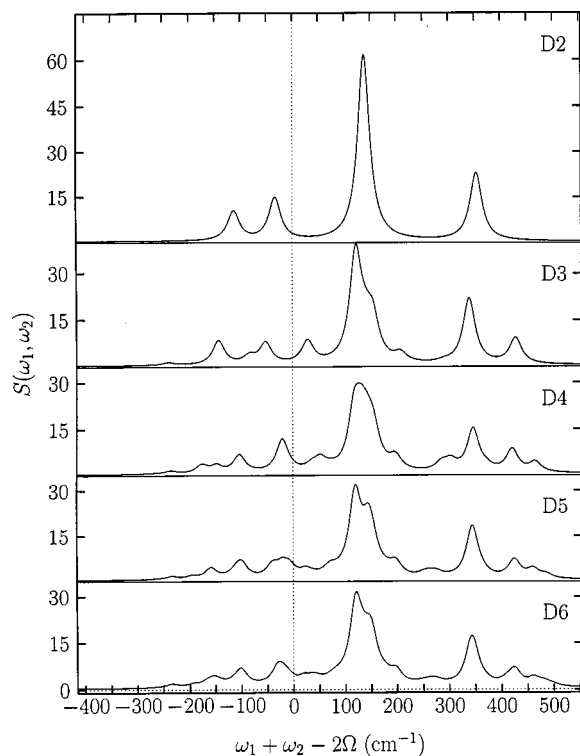


FIG. 7. Same as in Fig. 6 except that the dephasing rate is $\gamma \sim 15 \text{ cm}^{-1}$.

have a common origin at least one generation below (see Fig. 4). Also note the symmetry $\Psi_{\bar{\alpha}}(ij,p) = \Psi_{\bar{\alpha}}(ji,p)$.

Our calculations reveal that the strongest element $\Psi_{\bar{\alpha}}(ij,p)$ appears in general for periphery chromophores within the same branch, that is, $i, j \rightarrow l$ and $p \neq 0$. We further note that $\Psi_{\bar{\alpha}}(ii, i-1) = 0$ for $i > 1$ due to the following selection rule: $\text{Im}(Y_{ii, i-1}) = 0$ for $i > 1$. This describes the situation when two chromophores are the closest nearest neighbors in the same generation (except when they belong to different branches).

Figure 8(b) displays the wave function for the two-exciton band edge, i.e., the lowest (dark) state at $\Delta\omega \approx -260 \text{ cm}^{-1}$. This wave function is dominated by a single element $\Psi_{\bar{\alpha}}(44,3) = -5.45$, and is much more localized than the bright state at $\Delta\omega \approx 120 \text{ cm}^{-1}$ displayed in Fig. 8(a).

In order to show which parts of the molecule contribute to the $\Delta\omega \approx 120 \text{ cm}^{-1}$ resonance we display the product $n_{ij,p} \text{Im}(M_{ij,p} Y_{ij,p})$ in Fig. 9 using the same format of Fig. 8. (The statistical weights $n_{ij,p}$ of the distinct chromophore pairs are shown in Fig. 5.) The sum of these products [Eq. (13)] gives the signal. The dominant contribution comes from periphery chromophore pairs $[(i,j) = l-1, l]$ and the pairs located between the center and the periphery ($1 < (i,j) < l-1$) due to their exponentially large number [see Eqs. (12)]. The varying sign of the wave function leads to a huge cancellation between positive (left column) and negative (right column) contributions to the signal. Its magnitude is only 2%–5% of the positive or negative parts as shown in Fig. 10. As seen from Eq. (12), there are total $N = 127$ distinct chromophore pairs (with different $n_{ij,p}$) but only 67 are different [due to the symmetry in interchanging i and j indices in (ij,p) basis]. Each panel in Fig. 10 corresponds to one of the resonances of Fig. 6. We have ordered the positive and negative contributions separately in decreasing absolute magnitude. The figure displays the cumulative positive, negative contributions and their sum. The $\Delta\omega \approx 420, 340,$ and -35 cm^{-1} peaks converge at $N \sim 80$ whereas the $\Delta\omega \approx 120, -105 \text{ cm}^{-1}$ resonances converge at $N \sim 20$.

To further characterize the two-exciton wave functions we have computed three quantities, inverse participation ratio, average generation number, and the average distance between two distinct chromophores, which are plotted in Fig. 11.

To gauge the degree of localization of two-exciton states, we introduce the inverse participation ratio,^{5,17–19}

$$\langle P_{\bar{\alpha}} \rangle = \frac{\sum_{\bar{m} > \bar{n}} |\Psi_{\bar{\alpha}}(\bar{m}, \bar{n})|^2}{\sum_{\bar{m}, \bar{n}} |\Psi_{\bar{\alpha}}(\bar{m}, \bar{n})|^4}, \quad (14)$$

which using normalized $\Psi_{\bar{\alpha}}(\bar{m}, \bar{n})$ and Eq. (9), can be also recast in the form

$$\langle P_{\bar{\alpha}} \rangle = \frac{2(\sum_{ij,p} n_{ij,p} |\text{Im}(Y_{ij,p})|^2)^2}{\sum_{ij,p} n_{ij,p} |\text{Im}(Y_{ij,p})|^4}. \quad (15)$$

$\langle P_{\bar{\alpha}} \rangle = k$ indicates that the two-exciton wave function $\Psi(\bar{m}, \bar{n})$ is delocalized over k chromophore pairs. The maximum value $\langle P_{\bar{\alpha}} \rangle \equiv P_{\text{max}} = N(N-1)/2$ where $N = 3(2^l - 1)$ is the total number of chromophores in Dl .⁵ ($P_{\text{max}} = 17\,766$ in

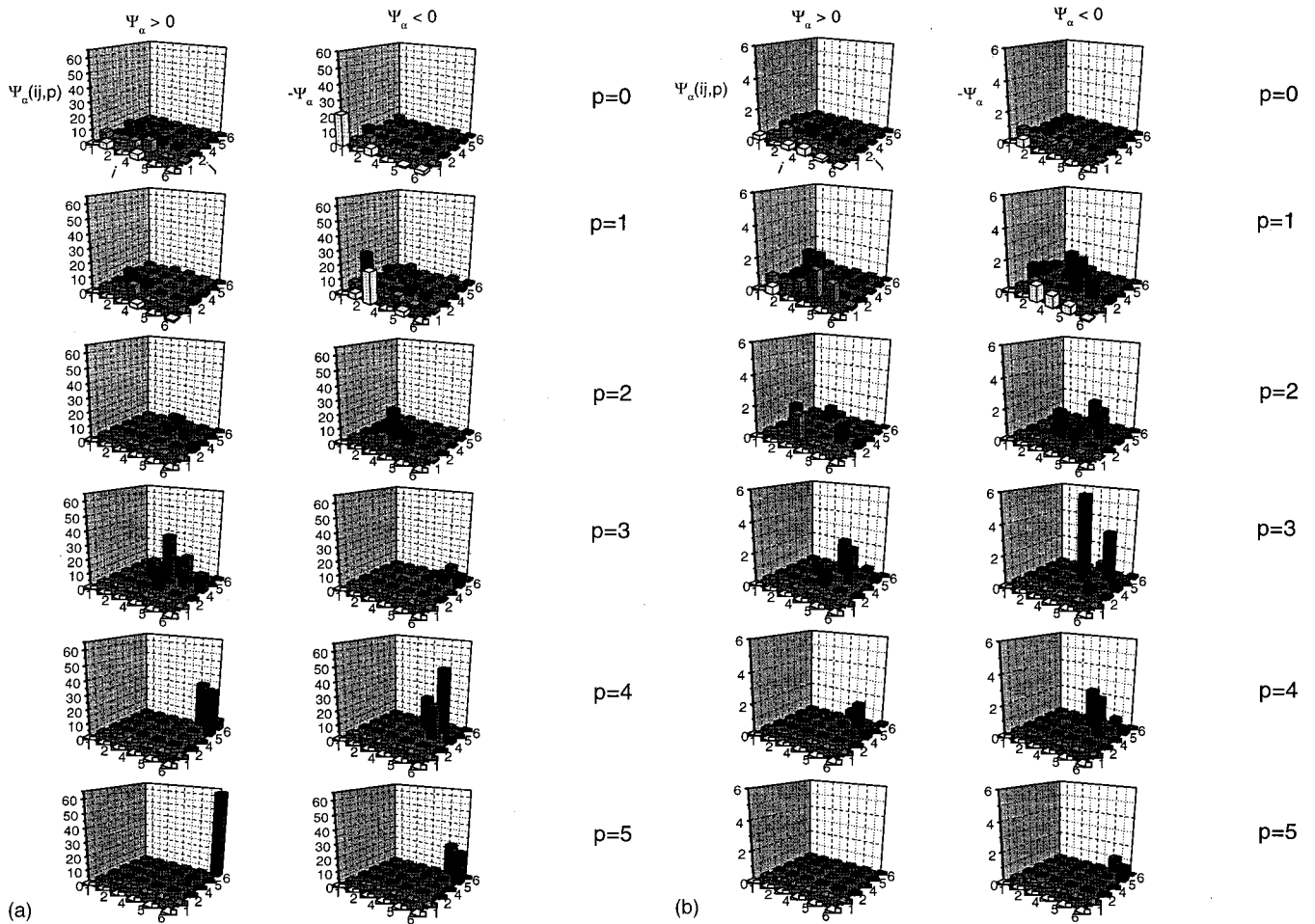


FIG. 8. (a) Two-exciton wave function $\Psi(\bar{m}, \bar{n})$ for D6 plotted in the basis (ij, p) for the major peak and the lowest energy state of $S(\omega_1, \omega_2)$ in Fig. 6 calculated with the shift $\Delta\omega = \omega_1 + \omega_2 - 2\Omega = 120 \text{ cm}^{-1}$. The left (right) column represents $\Psi > 0$ ($\Psi < 0$). Each row corresponds to different $p=0$ (top) and $p=5$ (bottom), i and j are the axes in the x - y plane. (b) same as (a) but for the lowest two-exciton state with $\Delta\omega = -260 \text{ cm}^{-1}$.

D6.) The minimum value $P_{\min}=1$ corresponds to the localization of the two-exciton state on a single chromophore pair ($N=2$).

In Fig. 11 (second panel from the top), we display the inverse participation ratio for the two-photon resonances. All the two-exciton states are clearly localized. The maximum localization with $\langle P_{\bar{\alpha}} \rangle \approx 304$ is of the major peak of $\Delta\omega = 120 \text{ cm}^{-1}$, so that the excitation is distributed on about seven distinct chromophore pairs. The maximum $\langle P_{\bar{\alpha}} \rangle \approx 8580$ on the band edge $\Delta\omega = 480 \text{ cm}^{-1}$ is still two times smaller than P_{\max} . The figure shows that more delocalized states (with higher $P_{\bar{\alpha}}$) appear at the red band edge. Two-exciton localization is different from the behavior of one-exciton states, which tend to be delocalized on both band edges.⁵

To analyze the signal's dependence on molecular connectivity, we plot the average generation number in Fig. 11.

This number, $\langle i_{\bar{\alpha}} \rangle = \sum_{\bar{m} > \bar{n}} |\bar{m}| |\Psi_{\bar{\alpha}}(\bar{m}, \bar{n})|^2$, is written using Eq. (9),

$$\langle i_{\bar{\alpha}} \rangle = \frac{\sum_{ijp} i n_{ij,p} |\text{Im}(Y_{ij,p})|^2}{\sum_{ijp} n_{ij,p} |\text{Im}(Y_{ij,p})|^2}. \quad (16)$$

Figure 11 shows that the average generation number varies between 3 and 5, which means that both the periphery chromophores and the intermediate chromophores (placed between periphery and the dendrimer center) contribute most strongly to the signal. This behavior can be rationalized using Fig. 9: The number of periphery chromophores grows exponentially compared to the center chromophores, and therefore the former dominate the two-exciton spectrum.

To quantify the relative motion of excitons in two-exciton states, we introduce the average distance between two chromophores \bar{i} and \bar{j} . This can be expressed in terms of their generation numbers and generation number of the branch origin to which both the chromophores belong,

$$r_{ij,p} = \frac{i+j-2p}{2}, \quad r_{ij,0} = \frac{i+j}{2} + 1. \quad (17)$$

Upon averaging of Eq. (17), we obtain

$$\langle R_{\bar{\alpha}} \rangle = \sum_{\bar{m} > \bar{n}} r_{\bar{m}\bar{n}} |\Psi_{\bar{\alpha}}(\bar{m}, \bar{n})|^2 = \frac{\sum_{ijp} r_{ij,p} n_{ij,p} |\text{Im}(Y_{ij,p})|^2}{\sum_{ijp} n_{ij,p} |\text{Im}(Y_{ij,p})|^2}. \quad (18)$$

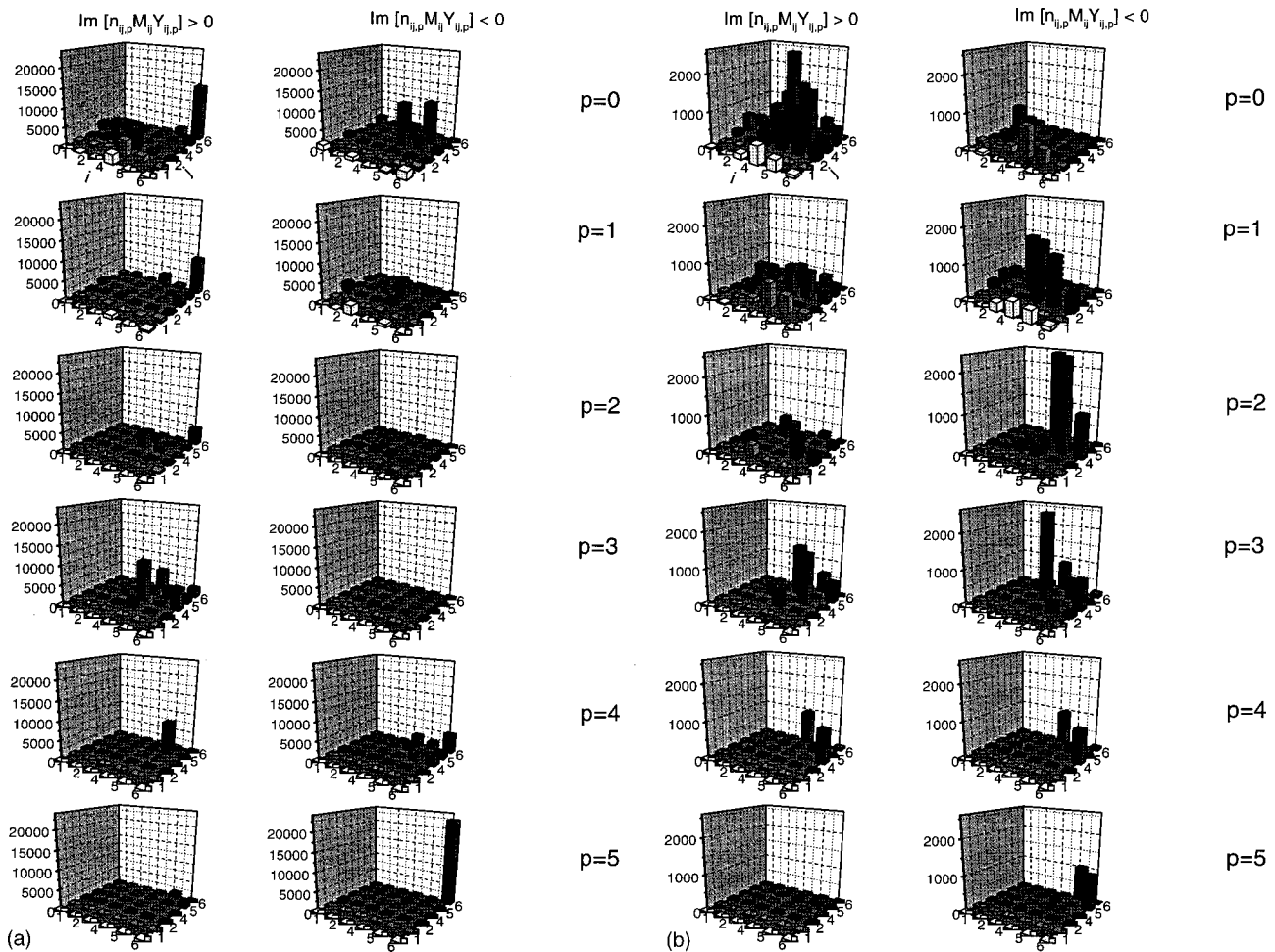


FIG. 9. Contributions to the two-photon resonances for D_6 : Imaginary part of $(n_{ij,p} M_{ij} Y_{ij,p})$ is plotted for $\Delta\omega = 120 \text{ cm}^{-1}$ [Fig. 9(a)] and $\Delta\omega = -260 \text{ cm}^{-1}$ [Fig. 9(b)]. The plots are organized in the same way as in Fig. 8.

The bottom panel in Fig. 11 shows that $1 \leq \langle R_{\bar{\alpha}} \rangle \leq 4$ in general, but $1 \leq \langle R_{\bar{\alpha}} \rangle \leq 2$ for the major absorption peaks in Fig. 6. This indicates that the main contributions to the signal come from nearest-neighbor chromophores, and the two-exciton coherence contributing to the signal is short range.

V. SUMMARY

In this paper we have investigated the two-exciton states which dominate the frequency-domain two-color four-wave mixing signal in compact dendrimers, computed in our earlier work.¹⁵ When both incoming frequencies are tuned off-resonant with respect to the one-exciton manifold, keeping the frequency sum on resonance with the two-exciton band, the signal can be expressed in terms of two-exciton states alone. This applies for a general Frenkel-exciton system. Averaging over the orientations of mixed waves with specifically chosen polarizations leads to a signal which does not depend on dipole orientations and reflects the exciton dynamics alone. The effective two-exciton dipole $d_{\bar{\alpha}}(\omega)$ which characterizes the two-exciton state contributions to the signal was expressed in terms of the two-exciton wave functions. The latter does not require the two-exciton states, and its calculation only involves matrices no larger than the $l \times l$

dimension with l being number of generations. To avoid the expensive direct diagonalization of the two-exciton Hamiltonian and to obtain information on the relevant two-exciton states, we have related the two-exciton wave functions $\Psi_{\bar{\alpha}}(\bar{m}, \bar{n})$ to the two-exciton coherence $Y_{\bar{m}\bar{n}}(\omega)$ at the resonance frequencies. The latter may be expressed in terms of the exciton scattering matrix $\bar{\Gamma}_{\bar{m}\bar{n}}(\omega)$, thus, relating the two-exciton wave functions to $\bar{\Gamma}_{\bar{m}, \bar{n}}(\omega)$. The two-exciton states which participate in signal by symmetry have been classified and mapped onto an effective model of a linear-chain system. The overall number of such states is $N^{(2)} = l(l^2 + 4l + 1)/6$.

Focusing on the five strongest resonances in the two-color four-wave mixing signal we have calculated the two-exciton coherences that completely describe their two-exciton wave function [see Eqs. (9) and (B3)–(B6)]. The special choice of the field polarizations in the four-wave mixing allows us to obtain this information irrespective of the chromophore (linear unit) orientation in space, which is complex in dendrimers with large l . The signal depends entirely on the segment's connectivity and internal chromophore interactions and is dominated by periphery chromophores.

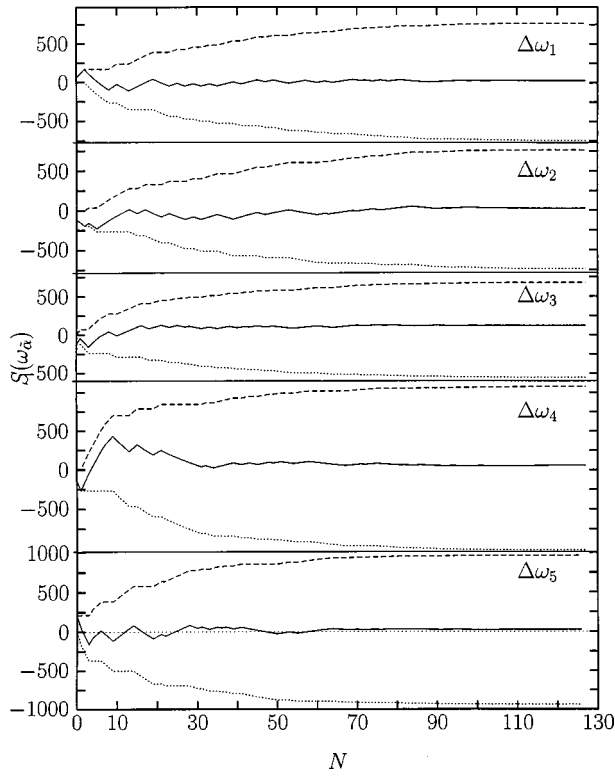


FIG. 10. Convergence of door-window representation $n_{ij,p} \text{Im}(M_{ij,p} Y_{ij,p})$ to the nonlinear signal (solid lines) as a function of number of distinct chromophore pairs. The dashed (dotted) lines represent the separate positive (negative) contributions to the signal. The five panels (from top to bottom) are given for the resonances at $\Delta\omega = 420, 340, 120, -35, -105 \text{ cm}^{-1}$.

ACKNOWLEDGMENTS

The support of the National Science Foundation and the U.S. Air Force Office of Scientific Research is gratefully acknowledged.

APPENDIX A: THIRD-ORDER SUSCEPTIBILITY OF CHROMOPHORE AGGREGATES

Below we express the third-order optical susceptibility $\hat{\chi}^{(3)}$ in terms of the one- and two-exciton eigenstates $\phi_{\bar{\alpha}}$ and $\Psi_{\bar{\alpha}}$ using the standard sum-over-states expression.¹² Assuming that the detunings of ω_1 and ω_2 from the one-exciton manifold are large compared to the exciton bandwidth but small compared to the transition frequency, we can invoke the rotating-wave approximation. This yields

$$\begin{aligned} \hat{\chi}^{(3)}(-\omega_2; \omega_1, \omega_2, -\omega_1) &= \sum_{\bar{\alpha}\bar{\beta}\bar{\gamma}} \frac{\langle g | P \cdot \hat{e}_3 | \bar{\beta} \rangle \langle \bar{\beta} | P \cdot \hat{e}_3 | \bar{\gamma} \rangle \langle \bar{\gamma} | P \cdot \hat{e}_1 | \bar{\alpha} \rangle \langle \bar{\alpha} | P \cdot \hat{e}_1 | g \rangle}{\omega_1 + \omega_2 - \epsilon_{\bar{\gamma}} + i\gamma} \\ &\times \left[\frac{1}{\omega_1 - \epsilon_{\bar{\alpha}} + i\gamma/2} + \frac{1}{\omega_2 - \epsilon_{\bar{\alpha}} + i\gamma/2} \right] \\ &\times \left[\frac{1}{\omega_1 - \epsilon_{\bar{\beta}} - i\gamma/2} + \frac{1}{\omega_2 - \epsilon_{\bar{\beta}} + i\gamma/2} \right], \end{aligned} \quad (\text{A1})$$

where polarization operator P is

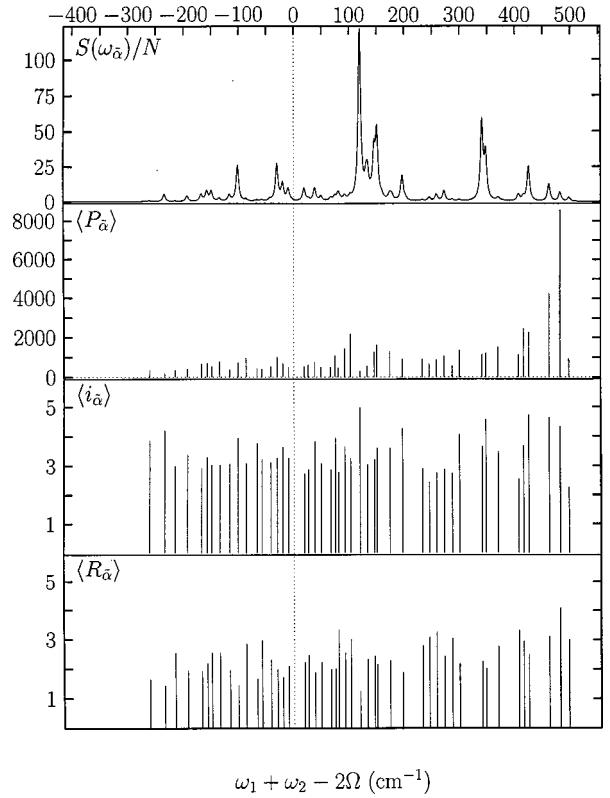


FIG. 11. Signal dependence in D6. From top to bottom: The high-resolution signal, the inverse participation ratios $\langle P_{\bar{\alpha}} \rangle$, the average generation number $\langle i_{\bar{\alpha}} \rangle$, and the average distance between chromophore pairs $\langle R_{\bar{\alpha}} \rangle$.

$$P = \sum_{\bar{m}} \mu_{\bar{m}} (B_{\bar{m}}^{\dagger} + B_{\bar{m}}). \quad (\text{A2})$$

Here $\epsilon_{\bar{\alpha}}$ and ϵ_{gg} stand for the energies of one- and two-exciton eigenstates, respectively, and $\gamma/2$ denotes the exciton dephasing rate. The one-exciton states can be eliminated from Eq. (A1) by detuning ω_1 and ω_2 off the one-exciton band ($\omega_1 + \omega_2 \approx 2\Omega$ is resonant with the two-exciton manifold). We can set $\omega_1 - \epsilon_{\bar{\alpha}} + i\gamma/2 \approx \omega_1 - \Omega$, $\omega_2 - \epsilon_{\bar{\alpha}} + i\gamma/2 \approx -(\omega_1 - \Omega)$ in the denominator of the resulting expression. Equation (A1) then assumes the form

$$\begin{aligned} \text{Im}[\hat{\chi}^{(3)}] &= \frac{1}{(\omega_1 - \Omega)^4} \sum_{\bar{\alpha}} d_{\bar{\alpha}}^{(3)}(\omega) d_{\bar{\alpha}}^{(1)}(\omega) \\ &\times \frac{\gamma}{(\omega - \epsilon_{\bar{\alpha}})^2 + \gamma^2}, \end{aligned} \quad (\text{A3})$$

where γ is the two-exciton dephasing rate, $\omega = \omega_1 + \omega_2$, and

$$d_{\bar{\alpha}}^{(j)}(\omega) \equiv \langle \bar{\alpha} | P_{\text{eff}}^{(j)}(\omega) | g \rangle \quad (\text{A4})$$

is the matrix element of an effective polarization operator which directly connects the ground state and the two-exciton manifold. $d_{\bar{\alpha}}^{(j)}$ are real since the one-exciton wave functions are real.⁵ The effective polarization operator has the form

$$P_{\text{eff}}^{(j)}(\omega) \equiv P \cdot \hat{e}_j (\omega - 2H) P \cdot \hat{e}_j. \quad (\text{A5})$$

APPENDIX B: TWO-EXCITON COHERENCE AND THE TWO-EXCITON WAVE FUNCTION

In this Appendix we relate two-exciton states with two-exciton variable $Y_{\bar{m}\bar{n}}$ for an arbitrary aggregate described by the Frenkel-exciton model. To that end we evaluate $Y_{\bar{m}\bar{n}}(\omega)$ for the system driven by two monochromatic fields in two ways.

The first procedure is based on the sum-over-states similar to that of the signal presented in Sec. II [see Eqs. (5) and (6)], and yields for $Y_{\bar{m}\bar{n}}$ averaged over the polarization directions,

$$Y_{\bar{m}\bar{n}}(\omega) = \frac{1}{(\omega_1 - \Omega)^2} \sum_{\bar{\alpha}} d_{\bar{\alpha}}(\omega) \frac{\gamma}{(\omega - \epsilon_{\bar{\alpha}}) + i\gamma} \Psi_{\bar{\alpha}}(\bar{m}, \bar{n}), \quad (\text{B1})$$

where $\Psi_{\bar{\alpha}}(\bar{m}, \bar{n})$ is given by Eq. (7), $\omega = \omega_1 + \omega_2$, and a numerical factor given by the product of the amplitudes of the waves is omitted.

$Y_{\bar{m}\bar{n}}$ may be alternatively obtained by solving the equation of motion for one- and two-exciton variables and expressing the solution in terms of the one- and two-exciton Green functions, followed by representing the latter in terms of $\bar{\Gamma}$ using the Bethe–Salpeter equation.²⁰ This yields

$$Y_{\bar{m}\bar{n}}(\omega) = \frac{1}{(\omega_1 - \Omega)^2} \sum_{\bar{n}'\bar{n}''} \bar{\Gamma}_{\bar{n}'\bar{n}''}(\omega) \times \sum_{\bar{\alpha}\bar{\beta}} \frac{\phi_{\bar{\alpha}}(\bar{n}') \phi_{\bar{\beta}}(\bar{n}'')}{\omega - \epsilon_{\bar{\alpha}} - \epsilon_{\bar{\beta}} + i\gamma} \phi_{\bar{\alpha}}(\bar{m}) \phi_{\bar{\beta}}(\bar{n}), \quad (\text{B2})$$

where $\phi_{\bar{\alpha}}(\bar{m})$ are the one-exciton wave functions.

By comparing the two expressions for $Y(\omega)$, one can express the two-exciton wave function in terms of $\bar{\Gamma}$. Equation (B1) gives $Y(\omega)$ in a form of a sum over resonances. When the dephasing rate γ is smaller than the spacing between the two-exciton levels, the resonances are well separated. Provided the two-exciton states are nondegenerate, and combining Eq. (B1) with Eqs. (5) and (6), we obtain Eq. (B2). It implies that $\text{Im}[Y_{\bar{m}\bar{n}}(\omega)]$ gives the two-exciton wave function $\Psi_{\bar{\alpha}}(\bar{m}, \bar{n})$ up to a numerical factor.

Below we apply the general expression for two-exciton coherence using the one-exciton states [Eq. (B2)] to the dendrimers. It follows from the symmetry of one-exciton states that the nonzero contributions to the sum over $\bar{\alpha}$ and $\bar{\beta}$ in Eq. (B2) come from pairs of excitons which are either both symmetric or both antisymmetric and have the same length. Expressing the one-exciton wave functions $\phi_{\bar{\alpha}}$ in Eq. (B2) in terms of linear-chain wave functions $\psi_{\bar{\alpha}}$ (by using transformation in Ref. 5), we could separate symmetric and antisymmetric terms following the steps of Ref. 15,

$$Y_{ij,p}(\omega) = Y_{ij,p}^S(\omega) + Y_{ij,p}^A(\omega), \quad (\text{B3})$$

where the contributions from pairs of antisymmetric excitons are given by

$$Y_{ij,p}^A(\omega) = \frac{(\omega_1 - \Omega)^{-2}}{\sqrt{2^{i+j}}} \sum_{s=1}^p 2^s (1 - 2\delta_{sp}) \times \sum_{\alpha,\beta=1}^{l-s} \psi_{\alpha}^{(l-s)}(i-s) \psi_{\beta}^{(l-s)}(j-s) \times \frac{\sum_{k=s+1}^l \bar{\Gamma}_k(\omega) \psi_{\alpha}^{(l-s)}(k-s) \psi_{\beta}^{(l-s)}(k-s)}{\omega - \epsilon_{\alpha}^{(l-s)} - \epsilon_{\beta}^{(l-s)} + i\gamma}, \quad p < \min\{i, j\}, \quad (\text{B4})$$

and

$$Y_{ij,j}^A(\omega) = \frac{(\omega_1 - \Omega)^{-2}}{\sqrt{2^{i+j}}} \sum_{s=1}^{j-1} 2^s \sum_{\alpha,\beta=1}^{l-s} \psi_{\alpha}^{(l-s)}(i-s) \times \psi_{\beta}^{(l-s)}(j-s) \times \frac{\sum_{k=s+1}^l \bar{\Gamma}_k(\omega) \psi_{\alpha}^{(l-s)}(k-s) \psi_{\beta}^{(l-s)}(k-s)}{\omega - \epsilon_{\alpha}^{(l-s)} - \epsilon_{\beta}^{(l-s)} + i\gamma}, \quad (\text{B5})$$

and from symmetric excitons

$$Y_{ij,p}^S(\omega) = \frac{2(\omega_1 - \Omega)^{-2}}{3\sqrt{2^{i+j}}} \sum_{\alpha,\beta=1}^l \sum_{t=1}^2 t(Q_p)^{t-1} \tilde{\psi}_{\alpha}^{(t)}(i) \times \tilde{\psi}_{\beta}^{(t)}(j) \frac{\sum_{k=1}^l \bar{\Gamma}_k(\omega) \tilde{\psi}_{\alpha}^{(t)}(k) \tilde{\psi}_{\beta}^{(t)}(k)}{\omega - \epsilon_{\alpha,t} - \epsilon_{\beta,t} + i\gamma}, \quad (\text{B6})$$

where $Q_p = 1$ for $p \neq 0$ ($Q_p = -1/2$ for $p = 0$) implies that two chromophores belong to the same (different) branch.

Using the results of Sec. II, the two-exciton wave functions are given by $\text{Im}[Y_{\bar{m}\bar{n}}(\omega_{\bar{\alpha}})]$, where $\omega_{\bar{\alpha}}$ denote the peak positions of the nonlinear signal. Equations (B3)–(B6) constitute then closed-form expressions for the two-exciton wave functions.

Alternatively, the window wave function $M_{\bar{i}\bar{j}}$ can be represented by a matrix $M_{ij,p}$ which has the form

$$M_{ij,p}(\omega) = (\omega - 2\Omega - 4J) + 2J(\delta_{i,1} + \delta_{j,1} + \delta_{i,l} + \delta_{j,l}). \quad (\text{B7})$$

APPENDIX C: SYMMETRIC TWO-EXCITON STATES OF DENDRIMERS

In this Appendix we derive a Hamiltonian for the two-exciton states which are symmetric with respect to G_l and are the only states that contribute in the four-wave mixing signal. We denote the basis set $X_l^{(2)}$ for all two-exciton states as the set of pairs (\bar{i}, \bar{j}) with $\bar{i} \neq \bar{j}$, $\bar{i} \geq \bar{j}$. The pairs (\bar{i}, \bar{j}) and (\bar{j}, \bar{i}) for $|\bar{i}| = |\bar{j}|$ should be identical. This results from the fact that the two-exciton wave functions $\Psi(\bar{i}, \bar{j})$ are symmetric with respect to permutations of \bar{i} and \bar{j} and vanish for $\bar{i} = \bar{j}$. We further introduce a set of subsets $A_{ij,p} \subset X_l^{(2)}$ of the two-exciton basis set with $l, j = 1, \dots, l$; $p = 0, 1, \dots, l-1$; $p \leq j \leq i$, and for $i = j, p < j$. $A_{ij,p}$ is defined as a set of pairs $(\bar{i}, \bar{j}) \in X_l^{(2)}$ with $|\bar{i}| = i$, $|\bar{j}| = j$, and $|\bar{p}(\bar{i}, \bar{j})| = p$, which means that $A_{ij,p}$ is represented by pairs of chromophores which belong to the generations i and j with the intersection point lying in the generation p . By definition, the subsets

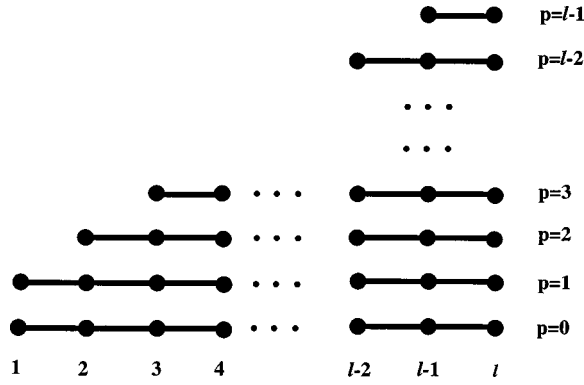


FIG. 12. The effective lattice model for double excitations in dendrimer: Collection of linear chains of variable length $p=0,1,\dots,l-1$.

$A_{ij,p}$ do not intersect, i.e., $A_{ij,p} \cap A_{i'j',p'} \neq \emptyset$ only for $i=i', j=j'$, and $p=p'$ and over $X_l^{(2)}$, i.e., $\cup A_{ij,p} = X_l^{(2)}$. This implies that the space of two-exciton states $W_l^{(2)}$ can be decomposed onto a direct sum of the vector spaces $W_{ij,p}^{(2)}$ spanned into the sets $A_{ij,p} : W_l^{(2)} = \oplus_{ijp} W_{ij,p}^{(2)}$. Using this notation, we can describe the symmetric (with respect to G_l) two-exciton states as those states whose wave functions are constants within each $A_{ij,p}$. A symmetric two-exciton state is described by a set of numbers $\Psi_{ij,p}$ representing the values of the wave functions on the elements of $A_{ij,p}$,

$$|\Psi\rangle = \sum_{ijp} \Psi_{ij,p} C_{ij,p} \sum_{(\bar{i}, \bar{j}) \in A_{ij,p}} B_{\bar{i}}^\dagger B_{\bar{j}}^\dagger |g\rangle, \quad (C1)$$

where the summation over i, j , and p satisfies the restrictions introduced in the definition of $A_{ij,p}$, and the normalization factors $C_{ij,p}$ are such that the states

$$|ij,p\rangle \equiv C_{ij,p} \sum_{(\bar{i}, \bar{j}) \in A_{ij,p}} B_{\bar{i}}^\dagger B_{\bar{j}}^\dagger |g\rangle, \quad (C2)$$

form an orthonormal basis set in the space of symmetric with respect to G_l two-exciton states. The normalization factors have the form $C_{ij,p} = 1/\sqrt{n_{ij,p}}$, where $n_{ij,p}$ was defined by Eq. (12).

The effective Hamiltonian H_{eff} for symmetric two-exciton states can be obtained by projecting the Frenkel exciton Hamiltonian [Eq. (1)] onto the subspace of relevant states determined by Eq. (A1). To visualize the structure of the effective Hamiltonian we decompose the space of symmetric two-exciton states $W_0^{(2)}$ into the direct sum $W_0^{(2)} = \oplus_{p=0}^{l-1} W_{0,p}^{(2)}$, where $W_{0,p}^{(2)}$ is generated by the states $|ij,p\rangle$ with the given p and $i, j=p, \dots, l, i \leq j$ (if $i=j$, then $i \neq p$). The space $W_{0,p}^{(2)}$ for $p \neq 0$ can be considered as the space of two-particle states on a linear chain of length $l-p-1$ with the sites $i=p, p+1, \dots, l$. Two excitations are allowed to reside on the same site except for $i=j=p$. For $p=0$ the effective chain of length l covers the sites $i=1, \dots, l$ with no restrictions with respect to the double occupancy. The effective lattice model is presented schematically in Fig. 12, and is represented by a collection of linear chains parameterized by $p=0, 1, \dots, l-1$. Both excitations can reside on the same chain only. The Hamiltonian can be partitioned into

intrachain terms which describe the two-particle dynamics within the chains and interchain terms which allow hopping of both the excitations onto the nearest-neighbor chains,

$$H_{\text{eff}} = \sum_{p=0}^{l-1} H_p^{(0)} + \sum_{p=0}^{l-2} H_{p,p+1}^{(\text{int})}. \quad (C3)$$

A straightforward calculation yields for $H_p^{(0)}$,

$$H_p^{(0)} = \sum_{j=p+2}^l (\Omega - J) B_{p,j}^\dagger B_{p,j} + \Omega (B_{p,p+1}^\dagger B_{p,p+1} + B_{p,p}^\dagger B_{p,p}) + \sum_{j=p+1}^{l-1} J\sqrt{2} (B_{p,j+1}^\dagger B_{p,j} + B_{p,j}^\dagger B_{p,j+1}) + J (B_{p,p+1}^\dagger B_{p,p} + B_{p,p}^\dagger B_{p,p+1}), \quad (C4)$$

whereas $H_0^{(0)}$ has the form

$$H_0^{(0)} = \sum_{j=1}^l (\Omega - J) B_{0,j}^\dagger B_{0,j} + \sum_{j=1}^{l-1} J\sqrt{2} (B_{0,j+1}^\dagger B_{0,j} + B_{0,j}^\dagger B_{0,j+1}), \quad (C5)$$

where $B_{p,j} (B_{p,j}^\dagger)$ is the annihilation (creation) operator on the site j in chain of length p . They satisfy the following commutation relations;

$$[B_{p,i}, B_{q,j}^\dagger] = \delta_{pq} \delta_{ij}, \quad \text{for } i \neq p, j \neq q,$$

$$[B_{p,p}, B_{q,q}^\dagger] = \delta_{pq} (1 - B_{p,p}^\dagger B_{p,p}). \quad (C6)$$

Equations (C6) imply that for any chain p the sites $j=p+1, \dots, l$ are represented by harmonic oscillators whereas the site $j=p$ is represented by a two-level system. The $p=0$ chain represents a system of bosons with the nearest-neighbor hopping, whereas for $p \neq 0$ we have a system of oscillators coupled to a two-level system. The evaluation of terms $H_{p,p+1}^{(\text{int})}$ which represent the coupling between the chains yields

$$H_{p,p+1}^{(\text{int})} = J \sum_{j=p+2}^l (B_{p+1,p+1}^\dagger B_{p+1,j}^\dagger B_{p,p} B_{p,j} + B_{p,p}^\dagger B_{p,j}^\dagger B_{p+1,p+1} B_{p+1,j}) - J \sum_{j=p+2}^l (B_{p+1,p+1}^\dagger B_{p+1,j}^\dagger B_{p,p+1} B_{p,j} + B_{p,p+1}^\dagger B_{p,j}^\dagger B_{p+1,p+1} B_{p+1,j}), \quad (C7)$$

$$H_{0,1}^{(\text{int})} = -J \sum_{j=2}^l (B_{1,1}^\dagger B_{1,j}^\dagger B_{0,1} B_{0,j} + B_{0,1}^\dagger B_{0,j}^\dagger B_{1,1} B_{1,j}). \quad (C8)$$

Equations (C7) and (C8) clearly show that the interchain hopping processes are allowed for the symmetric two-exciton states of the dendrimer. A double excitation $|ij,p\rangle$, which occupies the sites i and j on chain p with $i > j$, can hop

onto the nearest-neighbor chains $p-1$ and $p+1$ only if $j=p$ or $j=p+1$. The excitation i hops onto the same site of the neighboring chain, whereas the excitation j hops either onto the edge site of the neighbor chain or onto the same site (i.e., j), provided that j is the edge, or next to the edge, site on the new chain.

Finally, we compute the total number of symmetric two-exciton states. The chain p with $p \neq 0$ has $[(l-p+1)(l-p+2)/2-1]$ double excitations which is given by the number of two-particle boson states on the chain of length $l-p+1$ minus one, since a double excitation on the edge site is not allowed. The $p=0$ chain gives $l(l+1)/2$ double excitations since all sites are represented by bosons. Summation of the numbers of double excitations over the chains $p=0,1,\dots,l-1$ yields the overall number $N^{(2)}=l(l^2+4l+1)/6$.

¹M. R. Shortreed, S. F. Swallen, Z.-Y. Shi, W. Tan, Z. Xu, J. S. Moore, and R. Kopelman, *J. Phys. Chem. B* **101**, 6318 (1997).

²R. Kopelman, M. R. Shortreed, Z.-Y. Shi, W. Tan, Z. Xu, C. Devadoss, J. S. Moore, A. Bar-Haim, and Y. Klafter, *Phys. Rev. Lett.* **78**, 1239 (1997).

³M. Shortreed, Z.-Y. Shi, and R. Kopelman, *Mol. Cryst. Liq. Cryst. Sci. Technol., Sect. A* **283**, 95 (1996).

⁴C. Devadoss, P. Bharathi, and J. S. Moore, *J. Am. Chem. Soc.* **118**, 9635 (1996).

⁵E. Y. Poliakov, V. Chernyak, S. Tretiak, and S. Mukamel, *J. Chem. Phys.* **110**, 8161 (1999).

⁶Z. Xu, M. Kahr, K. L. Walker, C. L. Wilkins, and J. S. Moore, *J. Am. Chem. Soc.* **116**, 4537 (1994).

⁷D. A. Tomalia, A. M. Naylor, and W. A. Goddard, *Angew. Chem. Int. Ed. Engl.* **29**, 138 (1990).

⁸M. K. Lothian-Tomalia, D. M. Hedstrand, D. A. Tomalia, A. B. Padias, and H. K. Hall, Jr., *Tetrahedron* **53**, 15495 (1997).

⁹S. Tretiak, V. Chernyak, and S. Mukamel, *J. Phys. Chem. B* **102**, 3310 (1998).

¹⁰A. S. Davydov, *Theory of Molecular Excitons* (Plenum, New York, 1997).

¹¹*Excitons*, edited by E. I. Rashba and M. D. Sturge (North-Holland, Amsterdam, 1982); V. B. Brode, E. I. Rashba, and E. F. Sheka, *Spectroscopy of Molecular Excitons* (Springer, Berlin, 1985).

¹²S. Mukamel, *Principles of Nonlinear Optical Spectroscopy* (Oxford University Press, Oxford, 1995).

¹³*J-aggregates*, edited by T. Kobayashi (World Scientific, Singapore, 1996).

¹⁴*J. Phys. Chem. B* (Special issue on Light-Harvesting Physics Workshop), **101**, 7197-7359 (1997); V. Sundström and R. van Grondelle, in *Anoxygenic Photosynthetic Bacteria*, edited by R. E. Blankenship, M. T. Madiga, and C. E. Baner (Kluwer Academic, Dordrecht, 1995), p. 349.

¹⁵V. Chernyak, E. Y. Poliakov, S. Tretiak, and S. Mukamel, *MRS Proceedings*, edited by M. Drake and J. Klafter (in press).

¹⁶V. Chernyak and S. Mukamel, *Phys. Rev. B* **48**, 2470 (1993); *J. Chem. Phys.* **100**, 2974 (1994); V. Chernyak, N. Wang, and S. Mukamel, *Phys. Rep.* **263**, 213 (1995).

¹⁷E. N. Economou, *Green's Functions in Quantum Physics* (Springer, New York, 1994).

¹⁸D. Thouless, *Phys. Rep., Phys. Lett.* **13**, 93 (1974).

¹⁹F. C. Spano, J. R. Kuklinski, and S. Mukamel, *Phys. Rev. Lett.* **65**, 211 (1990).

²⁰V. Chernyak, W. M. Zhang, and S. Mukamel, *J. Chem. Phys.* **109**, 9587 (1998).